Radiation From a Hertzian Dipole Embedded in a Wire-Medium Slab

Yang Li, *Member, IEEE*, and Mário G. Silveirinha, *Member, IEEE*

***Abstract*—The radiated field expression for a short vertical electric dipole embedded in a wire-medium slab is derived using an effective medium approach. The dispersion characteristic equation of wave modes is presented, and the propagation and attenuation constants of each propagating mode are determined. Both a surface wave and a leaky wave are shown to propagate in the wire-medium slab. Near- and far-field distributions of the wave modes are computed and compared to full-wave simulation results.**

***Index Terms*—Effective medium theory, leaky wave, propagation, radiation, surface wave, wire-medium slab.**

I. Introduction

A WIRE-MEDIUM slab, also known as metal cut-wire array, refers to a Fakir's bed of nails substrate formed by perfect electric conductor (PEC) wires. The structure has received considerable attention in recent years for its applications as a negative-permittivity (ENG) metamaterial and electromagnetic band-gap (EBG) structure [1], [2]. Previously, researchers have investigated wave propagation in the wire-medium slab by solving a scattering problem with plane-wave incidence upon the slab [3] or by solving a source-free spectral problem [4]. In either way, the dispersion equation of wave modes was derived, and propagation mechanisms were identified. However, the theoretical problem of radiation from a dipole source in the wire-medium slab remains unsolved, and its solution can provide further physical insights into wave propagation and radiation in this structure.

In this letter, we set to characterize the radiation field of a vertical Hertzian dipole embedded in a wire-medium slab. In [5] and [6], Burghignoli *et al.* examined dipole source radiation from a different type of wire-medium slab using a transverse equivalent network representation and found that directive leaky-wave radiation can be achieved given the dipole excitation. In their wire-medium setup, the PEC wires are parallel to the air–slab interface, and as a result, no surface wave can be excited in the long wavelength regime. In our wire-medium slab, the PEC wires are perpendicular to the air–slab interface, and both surface wave and leaky wave can be supported along the structure.

Manuscript received December 19, 2012; revised February 23, 2013; accepted March 04, 2013. Date of publication March 19, 2013; date of current version April 04, 2013.

Y. Li is with the Department of Electrical and Computer Engineering, Baylor University, Waco, TX 76798 USA (e-mail: Yang_Li1@baylor.edu).

M. G. Silveirinha is with the Departamento de Engenharia Electrotécnica, Instituto de Telecomunicacões, Universidade de Coimbra, 3030 Coimbra, Portugal (e-mail: mario.silveirinha@co.it.pt).

Color versions of one or more of the figures in this letter are available online at http://ieeexplore.ieee.org.

Digital Object Identifier 10.1109/LAWP.2013.2253304

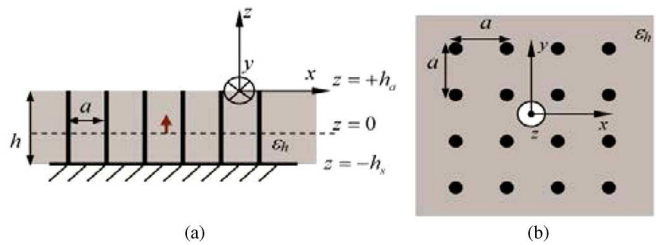

Fig. 1. Wire-medium slab setup. (a) Side view. (b) Top view.

This letter is organized as follows. In Section II, the radiation field from a dipole source in the wire-medium slab is formulated using an effective medium approach. The strong spatial dispersion inherent to the wire-medium is taken into account in the derivation. In Section III, the dispersion characteristic equation of wave modes is presented and solved. Both a surface wave and a leaky wave are shown to propagate in this structure at specific frequency bands. Near and far radiated electric fields are computed at different frequencies and locations. The results are compared to full-wave simulations. Section IV summarizes our findings.

II. Formulation of the Problem

Fig. 1 shows the wire-medium slab geometry setup. The wire height and spacing between wires are h and a, respectively. The source embedded inside the slab is a vertical Hertzian dipole with current density $\vec{J}$ ($\vec{J} = j\omega p_{\rm e}\delta(x)\delta(y)\delta(z)\hat{z}$, where $p_{\rm e}$ represents the electric dipole moment $q\ \vec{l}$). The dipole is placed at height $h_{\rm s}$ above the ground plane, and at height $h_{\rm a}$ below the air–slab interface. The permittivity of the host medium is $\varepsilon_{\rm h}$.

To find the radiation field from the dipole source, we first define an intermediate potential function Φ, using the electric field $\vec{E}$ that can be expressed as

$$\frac{\vec{E}}{p_{\rm e}} = \omega^2\mu_o\Phi\hat{z} + \frac{1}{\varepsilon_h}\nabla\left(\frac{\partial\Phi}{\partial z}\right). \tag{1}$$

The potential function Φ is simply related to the magnetic vector potential A_z as $A_z = j\omega p_{\rm e}\Phi$ and can be found from its spectral-domain counterpart $\tilde{\Phi}$ by taking inverse Fourier transform. In a previous work [7], the spectral-domain potential function $\tilde{\Phi}$ for an unbounded PEC wire-medium (formed by infinitely long wires) was found to be $(1/2\gamma_{\rm TM})e^{-\gamma_{\rm TM}|z|}$, where $\gamma_{\rm TM} = \sqrt{k_{\rm p}^2 + k_{\|}^2 - k_{\rm h}^2}$ is the propagation constant of the transverse magnetic (TM) mode, k_p is the plasmonic cutoff wavenumber, $k_{\|} = \sqrt{k_x^2 + k_y^2}$, and $k_{\rm h} = \omega\sqrt{\mu_o\varepsilon_{\rm h}}$. Based on this finding, we first derive $\tilde{\Phi}$ for a half-space, infinitely long

wire medium (i.e., $h_{\rm a} \to \infty$ in Fig. 1(a)) using the method of images

$$\tilde{\Phi} = \frac{1}{2\gamma_{\rm TM}} e^{-\gamma_{\rm TM}|z|} + \frac{1}{2\gamma_{\rm TM}} e^{-\gamma_{\rm TM}|z+2h_{\rm s}|}. \tag{2}$$

Motivated by (2), the knowledge that both TM and TEM modes can be excited in the wire-medium slab, and the tangential electric field of the TEM and TM modes must vanish independently at the ground-plane level $z = -h_{\rm s}$ [3], [4], we propose the following $\tilde{\Phi}$ for the geometry of Fig. 1:

$$\begin{aligned}\tilde{\Phi} = {} & \frac{1}{2\gamma_{\rm TM}} e^{-\gamma_{\rm TM}|z|} + \frac{1}{2\gamma_{\rm TM}} e^{-\gamma_{\rm TM}|z+2h_{\rm s}|} \\ & + A_{\rm TEM}\cosh(\gamma_{\rm TEM}(z+h_{\rm s})) \\ & + B_{\rm TM}\cosh(\gamma_{\rm TM}(z+h_{\rm s})), \qquad z < h_{\rm a} \qquad (3.a) \\ \tilde{\Phi} = {} & T e^{-\gamma_0(z-h_{\rm a})}, \qquad z > h_{\rm a} \qquad (3.b)\end{aligned}$$

where $\gamma_{\rm TEM} = jk_{\rm h}$ is the propagation constant of the TEM mode, $\gamma_0 = \sqrt{k_\parallel^2 - k_0^2}$, and $A_{\rm TEM}, B_{\rm TM}$, and T are unknown coefficients that can be determined by imposing the following three boundary conditions at the slab–air interface $z = h_{\rm a}$.

1) The continuity of the tangential component of the magnetic field at the interface requires that Φ is continuous. Therefore

$$\begin{aligned}&\frac{1}{2\gamma_{\rm TM}}(e^{-\gamma_{\rm TM}|h_{\rm a}|} + e^{-\gamma_{\rm TM}|h_{\rm a}+2h_{\rm s}|}) \\ &\quad + A_{\rm TEM}\cosh(\gamma_{\rm TEM}h) + B_{\rm TM}\cosh(\gamma_{\rm TM}h) = T. \qquad (4.a)\end{aligned}$$

2) The continuity of the tangential components of the electric field at the interface requires that $(1/\varepsilon_{\rm h}(z))(\partial\Phi/\partial z)$ is continuous, which results in

$$\begin{aligned}&\frac{1}{2}(e^{-\gamma_{\rm TM}h_{\rm a}} + e^{-\gamma_{\rm TM}|h_{\rm a}+2h_{\rm s}|}) - A_{\rm TEM}\gamma_{\rm TEM}\sinh(\gamma_{\rm TEM}h) \\ &\qquad - B_{\rm TM}\gamma_{\rm TM}\sinh(\gamma_{\rm TM}h) = \frac{\varepsilon_{\rm h}}{\varepsilon_0}\gamma_0 T. \qquad (4.b)\end{aligned}$$

3) An additional boundary condition (ABC), which ensures that the microscopic current at the ends of the wires vanishes, is imposed [8]. The ABC is equivalent to state that $k_{\rm h}^2\Phi + (\partial^2\Phi/\partial z^2)$ is continuous at the interface, which yields

$$\begin{aligned}&\frac{\gamma_{\rm TM}}{2}(e^{-\gamma_{\rm TM}h_{\rm a}} + e^{-\gamma_{\rm TM}|h_{\rm a}+2h_{\rm s}|}) + A_{\rm TEM}\gamma_{\rm TEM}^2\cosh(\gamma_{\rm TEM}h) \\ &\qquad + B_{\rm TM}\gamma_{\rm TM}^2\cosh(\gamma_{\rm TM}h) = (\gamma_0^2 + k_0^2 - k_{\rm h}^2)T. \qquad (4.c)\end{aligned}$$

By solving the linear system (4), $A_{\rm TEM}, B_{\rm TM}$, and T can be found as shown at the bottom of the page, where $\gamma_h = \sqrt{k_\parallel^2 - k_h^2}$ and $Q = (1/2)(e^{-\gamma_{\rm TM}h_a} + e^{-\gamma_{\rm TM}|h_a+2h_s|})$. Furthermore, we note that $\tilde{\Phi} = \tilde{\Phi}(k_x, k_y)$ is only dependent on $k_\parallel = \sqrt{k_x^2 + k_y^2}$. Therefore, it is possible to compute Φ as follows:

$$\begin{aligned}\Phi &= \frac{1}{(2\pi)^2}\iint \tilde{\Phi} e^{-j(k_x x + k_y y)} dk_x dk_y \\ &= \frac{1}{2\pi}\int_0^\infty \tilde{\Phi}(k_\parallel) J_0(k_\parallel \rho) k_\parallel dk_\parallel \qquad (5)\end{aligned}$$

where $\rho = \sqrt{x^2 + y^2}$ and J_0 is the first-kind Bessel function. This completes the formulation of our problem. To find the fields radiated by the dipole, one needs to numerically evaluate the Sommerfeld-type integral in (5).

III. Radiated Near and Far Fields in Wire-Medium Slab

To validate the above derivations and illustrate how a wave propagates in a wire-medium slab, we compute dispersion characteristics and field distributions of natural modes at different frequencies and positions and compare the theoretical predictions to full-wave simulations. In this example, the wire height h, spacing between wires a, and wire radius r are set to be 9 cm, 6 cm, and 2.5 mm, respectively. The dipole source is placed at the ground level ($h_{\rm s} = 0$ cm, $h_{\rm a} = 9$ cm). The host medium is air with $\varepsilon_{\rm h} = \varepsilon_0$.

It can be shown that for the indicated structural parameters, a *surface wave* will propagate inside the slab below the quarter-wave wire-length resonance frequency 830 MHz, and an *improper forward complex leaky wave* will dominate at frequencies above the plasmonic cutoff frequency 1670 MHz [4].

$$A_{\rm TEM} = \frac{Q\left(\gamma_h^2 - \gamma_{\rm TM}^2\right)\left[\cosh\left(\gamma_{\rm TM}h\right) + \sinh(\gamma_{\rm TM}h)\right]}{\gamma_{\rm TEM}(\gamma_h^2-\gamma_{\rm TM}^2)\cosh(\gamma_{\rm TM}h)\sinh(\gamma_{\rm TEM}h) + \cosh(\gamma_{\rm TEM}h)\left[\frac{\varepsilon_h}{\varepsilon_0}\gamma_0(\gamma_{\rm TEM}^2-\gamma_{\rm TM}^2)\cosh(\gamma_{\rm TM}h) + \gamma_{\rm TM}(\gamma_{\rm TEM}^2-\gamma_h^2)\sinh(\gamma_{\rm TM}h)\right]}$$

$$B_{\rm TM} = Q\frac{-\left[\left(\gamma_h^2 - \gamma_{\rm TEM}^2\right) + \frac{\varepsilon_h}{\varepsilon_0}\frac{\gamma_0}{\gamma_{\rm TM}}\left(\gamma_{\rm TEM}^2 - \gamma_{\rm TM}^2\right)\right]\cosh(\gamma_{\rm TEM}h) - \frac{\gamma_{\rm TEM}}{\gamma_{\rm TM}}\left(\gamma_h^2 - \gamma_{\rm TM}^2\right)\sinh(\gamma_{\rm TEM}h)}{\gamma_{\rm TEM}(\gamma_h^2-\gamma_{\rm TM}^2)\cosh(\gamma_{\rm TM}h)\sinh(\gamma_{\rm TEM}h) + \cosh(\gamma_{\rm TEM}h)\left[\frac{\varepsilon_h}{\varepsilon_0}\gamma_0(\gamma_{\rm TEM}^2-\gamma_{\rm TM}^2)\cosh(\gamma_{\rm TM}h) + \gamma_{\rm TM}(\gamma_{\rm TEM}^2-\gamma_h^2)\sinh(\gamma_{\rm TM}h)\right]}$$

$$T = \frac{Q\left(\gamma_{\rm TEM}^2 - \gamma_{\rm TM}^2\right)\cosh(\gamma_{\rm TEM}h)[\cosh(\gamma_{\rm TM}h) + \sinh\left(\gamma_{\rm TM}\right)h]}{\gamma_{\rm TEM}(\gamma_h^2-\gamma_{\rm TM}^2)\cosh(\gamma_{\rm TM}h)\sinh(\gamma_{\rm TEM}h) + \cosh(\gamma_{\rm TEM}h)\left[\frac{\varepsilon_h}{\varepsilon_0}\gamma_0(\gamma_{\rm TEM}^2-\gamma_{\rm TM}^2)\cosh(\gamma_{\rm TM}h) + \gamma_{\rm TM}(\gamma_{\rm TEM}^2-\gamma_h^2)\sinh(\gamma_{\rm TM}h)\right]}$$

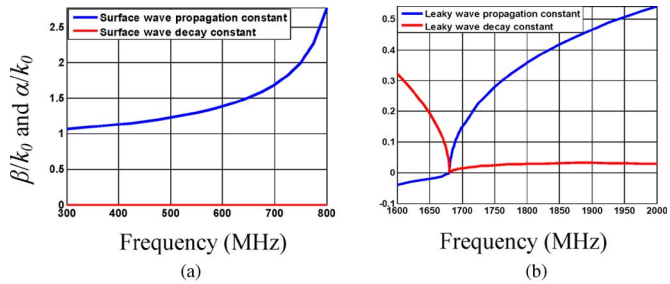

Fig. 2. Propagation characteristics. (a) Surface wave. (b) Leaky wave.

Below this frequency, the leaky wave becomes a *proper backward leaky mode*. Other branches of the surface wave can propagate in the leaky-wave regime, but since the leaky wave is dominantly excited, these are not discussed here. Moreover, complex wavenumbers ($k = \beta - j\alpha$) of both the surface- and leaky-wave modes can be computed by solving the following characteristic equation that corresponds to the pole of the integrand $\tilde{\Phi}$ in (5):

$$\gamma_{\mathrm{TEM}}\left(\gamma_{\mathrm{h}}^2 - \gamma_{\mathrm{TM}}^2\right)\tanh(\gamma_{\mathrm{TEM}}h) + \frac{\varepsilon_{\mathrm{h}}}{\varepsilon_0}\gamma_0\left(\gamma_{\mathrm{TEM}}^2 - \gamma_{\mathrm{TM}}^2\right) + \gamma_{\mathrm{TM}}\left(\gamma_{\mathrm{TEM}}^2 - \gamma_{\mathrm{h}}^2\right)\tanh\left(\gamma_{\mathrm{TM}}h\right) = 0. \quad (6)$$

Fig. 2(a) plots the normalized propagation constants β and attenuation constants α of the surface wave. It is clearly seen that the surface wave is a slow wave that propagates with $\beta > k_0$ and no attenuation in the limit of no loss. Fig. 2(b) plots both β and α of the leaky-wave poles with $\alpha > 0$. The symmetric leaky-wave poles (associated with $\alpha < 0$) are not shown here. Contrary to the surface wave, the leaky wave is a fast wave propagating with $|\beta| < k_0$ and nonnegligible decay, leaking energy out of the wire-medium slab.

The dipole radiated near and far fields in the wire-medium slab are computed by solving unknown coefficients $A_{\mathrm{TEM}}, B_{\mathrm{TM}}, T$ and evaluating the Sommerfeld integral (5). To avoid singularities of the integrand along the real axis, we detour the integration path on the upper half of the complex plane. First, the surface-wave near-field distribution is calculated at a sample frequency 600 MHz. Both E_z and E_x field components are shown in Fig. 3(a) and (b). In Fig. 3, the horizontal axis represents distance$x$ from the dipole source, and the vertical axis is the height z from the ground level. The color represents the normalized electric field strength on a decibel scale. Along the vertical direction, both E_z and E_x peak around the wire height level ($h = 9$ cm) and decay (exponentially) fast away from this interface.

To validate the theoretical results, we simulate near-field distributions for the same wire-medium slab using full-wave analysis tool FEKO [9]. The dipole source is placed at the center of a unit cell. As a finite-size wire-medium slab (54×54 in the xy-plane) is implemented in the simulation, there exists strong reflected wave from the end of the array. Such end-reflected waves are extracted using ESPRIT algorithm [10] and removed from the simulated fields to make fair comparison to theoretical results. The simulation results are exhibited in Fig. 3(c)

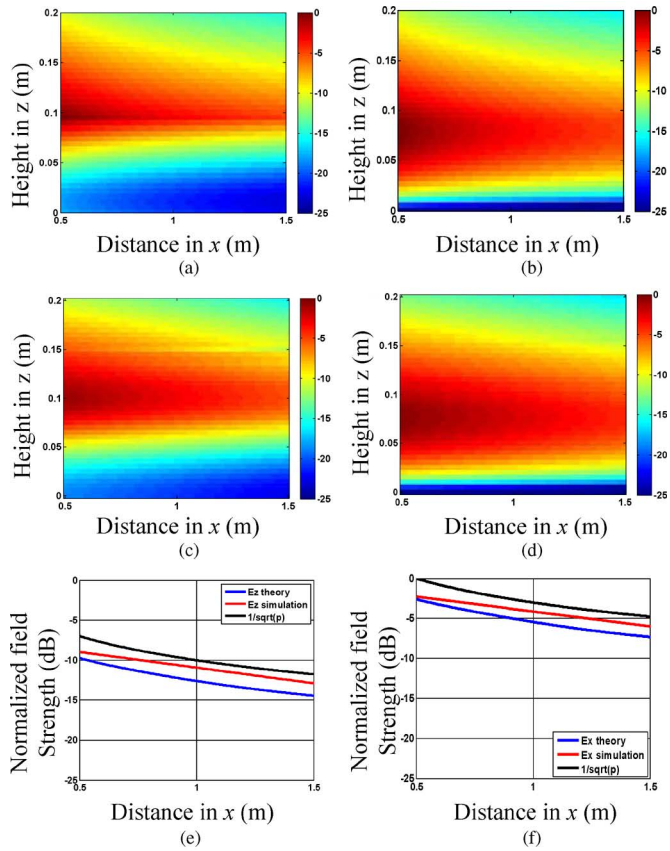

Fig. 3. Near electric field distributions at 600 MHz: (a) E_z theory; (b) E_x theory; (c) E_z simulation; (d) E_x simulation. (e) Comparisons of E_z at $z = 5$ cm. (f) Comparisons of E_x at $z = 5$ cm.

and (d). They are very similar to the theoretical predictions. To make more quantitative comparisons, the near electric fields are plotted against distance x at a sample height $z = 5$ cm and compared between theory and simulation in Fig. 3(e) and (f). Through slope comparison, it is seen that both components experience $1/\sqrt{\rho}$ range decay along the horizontal direction as result of the cylindrical wave expansion.

The dipole radiated field in the leaky-wave regime is also generated at a sample frequency 1800 MHz. Fig. 4 depicts the magnitudes of both E_z and E_x in the leaky-wave regime from the theory and the simulation. It is seen that both field components are strong inside the wire-medium slab. The wave propagates along the positive x-direction, but decays fast, leaking energy out of the slab. The results show good agreement between theory and simulation.

Finally, we investigate the far-field radiation patterns of the wire-medium slab with dipole excitation. While the surface-wave maximum radiation is always in the endfire direction, the far fields of leaky-wave radiation are more interesting and exhibit frequency scanning behavior. Fig. 5(a) plots the directivity patterns of the wire-medium slab in the elevation plane ($\phi = 0°$) at 1700, 1800, and 1900 MHz. It is seen that as frequency increases, the main beam shifts towards the endfire direction from $\theta = 15°$ to $\theta = 30°$. For comparison, the far-field radiation pattern is also simulated using FEKO. In this case, an infinite-size

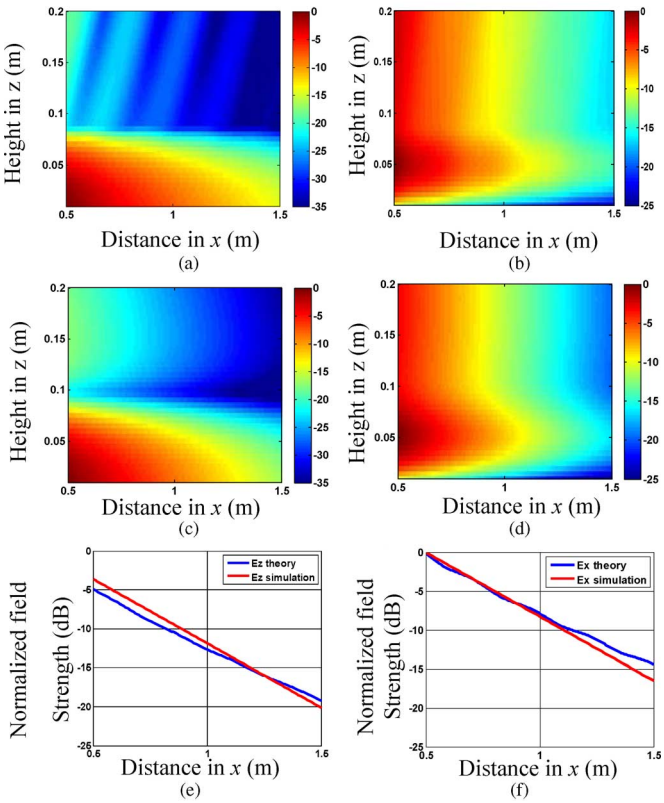

Fig. 4. Near electric field distributions at 1800 MHz: (a) E_z theory; (b) E_x theory; (c) E_z simulation; (d) E_x simulation. (e) Comparisons of E_z at $z = 5$ cm. (f) Comparisons of E_x at $z = 5$ cm.

wire-medium slab is modeled using a single unit cell with periodic boundary conditions on the sidewalls. A plane-wave excitation is launched for various incident angles, and E_z is calculated at the source location. By applying Lorentz reciprocity theorem [6], the far fields of the leaky wave can thus be obtained. The simulation results are shown in Fig. 5(b), where θ shifts from 22° at 1700 MHz to 35° at 1900 MHz, thus exhibiting similar frequency scanning behavior as in the theory predictions. The differences between the theory and full-wave simulation can be attributed to the upper frequency limit of the homogenization model. At 1700 MHz and above, the homogenization model may not work as well as in the low-frequency long-wavelength region since the granularity of the array is comparable to the guided wavelength and plays a relevant role in its electromagnetic response.

IV. Conclusion

In this letter, the radiated field from a vertical Hertzian dipole embedded in a wire-medium slab is characterized using an effective medium approach. The additional boundary condition is applied in the derivation, and the radiated fields are found in the form of a Sommerfeld-type integral.

We validate the field expressions by computing dispersion characteristics and field distributions of the wave modes in a wire-medium slab. It is shown that both surface wave and leaky wave can propagate in the structure. The propagation constants and attenuation constants of surface wave and leaky wave are calculated by solving the characteristic equation. Near- and far-field distributions of the wave modes are also computed and compared to full-wave numerical simulations. The results show a good agreement, particularly at low frequencies where the homogenization theory works well.

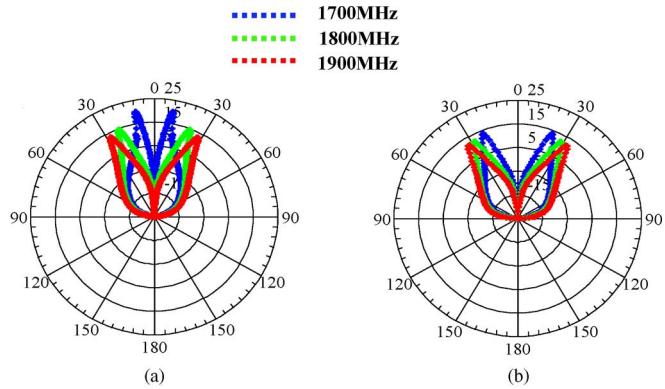

Fig. 5. Leaky-wave antenna directivities (on decibel scale) at 1700–1900 MHz. (a) Theory predictions. (b) Simulation results.

For future work, the authors are working on dipole radiation in a dielectric rod array slab, which has several potential applications in the context of metamaterials with exotic properties [11], and in understanding of wave propagation in forested environments [12].

References

[1] J. B. Pendry, A. J. Holden, W. J. Stewart, and I. Youngs, "Extremely low frequency plasmons in metallic mesostructures," *Phys. Rev. Lett.*, vol. 76, pp. 4773–4776, June 1996.

[2] S. Enoch, G. Tayeb, and B. Gralak, "The richness of the dispersion relation of electromagnetic bandgap materials," *IEEE Trans. Antennas Propag.*, vol. 51, no. 10, pp. 2659–2666, Oct. 2003.

[3] M. G. Silveirinha, C. A. Fernandes, and J. R. Costa, "Electromagnetic characterization of textured surfaces formed by metallic pins," *IEEE Trans. Antennas Propag.*, vol. 56, no. 2, pp. 405–415, Feb. 2008.

[4] A. B. Yakovlev, M. G. Silveirinha, O. Luukkonen, C. R. Simovski, I. S. Nefedov, and S. A. Tretyakov, "Characterization of surface-wave and leaky-wave propagation on wire-medium slabs and mushroom structures based on local and nonlocal homogenization models," *IEEE Trans. Microw. Theory Tech.*, vol. 57, no. 11, pp. 2700–2714, Nov. 2009.

[5] P. B. Burghignoli, G. Lovat, F. Capolino, D. R. Jackson, and D. R. Wilton, "Modal propagation and excitation on a wire-medium slab," *IEEE Trans. Microw. Theory Tech.*, vol. 56, no. 5, pp. 1112–1124, May 2008.

[6] P. B. Burghignoli, G. Lovat, F. Capolino, D. R. Jackson, and D. R. Wilton, "Directive leaky-wave radiation from a dipole source in a wire-medium slab," *IEEE Trans. Antennas Propag.*, vol. 56, no. 5, pp. 1329–1339, May 2008.

[7] M. G. Silveirinha and S. I. Maslovski, "Radiation from elementary sources in a uniaxial wire medium," *Phys. Rev. B*, vol. 85, p. 155125, Apr. 2012.

[8] M. G. Silveirinha, "Additional boundary condition for the wire medium," *IEEE Trans. Antennas Propag.*, vol. 54, no. 6, pp. 1766–1780, Jun. 2006.

[9] FEKO ver. 6.1, EM Software and Systems-S.A., Stellenbosch, South Africa, 2011 [Online]. Available: Http://www.emss.co.za

[10] Y. Li and H. Ling, "Extraction of wave propagation mechanisms in a cut-wire array using the ESPRIT algorithm," *IEEE Antennas Wireless Propag. Lett.*, vol. 8, pp. 744–747, 2009.

[11] K. Vynk, D. Felbacq, E. Centeno, A. I. Cabuz, D. Cassagne, and B. Guizal, "All-dielectric rod-type metamaterials at optical frequencies," *Phys. Rev. Lett.*, vol. 102, p. 133901, 2009.

[12] Y. Li and H. Ling, "Investigation of wave propagation in a dielectric rod array: Towards the understanding of HF/VHF propagation in a forest," *IEEE Trans. Antennas Propag.*, vol. 58, no. 12, pp. 4025–4032, Dec. 2010.